

Controlled generation and manipulation of vortex dipoles in a Bose-Einstein condensate

Tomohiko Aioi,¹ Tsuyoshi Kadokura,¹ Tetsuo Kishimoto,^{1,2,3} and Hiroki Saito¹

¹*Department of Engineering Science, University of Electro-Communications, Tokyo 182-8585, Japan*

²*Center for Frontier Science and Engineering, University of Electro-Communications, Tokyo 182-8585, Japan*

³*PRESTO, Japan Science and Technology Agency (JST), Saitama 332-0012, Japan*

(Dated: January 27, 2013)

We propose methods to generate and manipulate vortex dipoles in a Bose-Einstein condensate using Gaussian beams of red or blue-detuned laser. Velocity-controlled vortex dipoles are shown to be created and launched by a red-detuned beam and by two blue-detuned beams. Critical velocities for the vortex nucleation are investigated. The launched vortex dipoles can be trapped, curved, accelerated, and decelerated using Gaussian beams. Collisions between vortex dipoles are demonstrated.

PACS numbers: 03.75.Lm, 03.75.Kk, 67.85.De, 47.37.+q

I. INTRODUCTION

A vortex dipole is a pair of vortices with opposite circulations, which is a fundamental excitation in a two-dimensional (2D) fluid and plays a pivotal role in thermodynamic behavior of 2D systems [1, 2]. In superfluids, vortices are topological defects of the macroscopic wave function and a vortex dipole consists of a quantized vortex and antivortex, whose circulations are quantized to $\pm h/m$ with h and m being Planck's constant and the mass of a particle [3, 4]. Such a topological structure of a quantized vortex dipole has been observed in a Bose-Einstein condensate (BEC) of an atomic gas [5] and in an exciton-polariton condensate [6]. Recently, dynamics of vortex dipoles have directly been observed in oblate BECs [7–9].

In the experiments reported in Refs [5, 7], vortex dipoles were created by stirring a BEC with a blue-detuned laser beam. When the velocity of the beam exceeds a critical velocity, vortex-antivortex pairs are released from the density dip produced by the laser beam. The created vortex dipoles then move through the BEC and exhibit various interesting dynamics [7–10], which can be observed in real time using the technique developed by the Amherst group [8, 9]. Theoretical study on a moving potential in superfluids has so far been focused on drag force [11–14], vortex formation and shedding dynamics [15–17], critical velocity [18, 19], scaling laws [20], and potential oscillation [21]. In addition to these studies, it is important to establish methods for controlled generation and manipulation of vortex dipoles, which increases the range of experiments and leads to precise understanding of dynamical properties of vortex dipoles.

The aim of the present paper is to propose methods to generate and manipulate quantized vortex dipoles in a BEC using not only a single blue-detuned laser beam but also a red-detuned beam and multiple beams. We will show that dynamics of vortex dipole creation for a red-detuned beam (attractive potential for atoms) are quite different from those for a blue-detuned beam (re-

pulsive potential for atoms). We propose methods to create and launch vortex dipoles with a controlled velocity and angle using a red-detuned beam or two blue-detuned beams. We also show that two red-detuned beams can trap a vortex dipole between them. The trajectories of the launched vortex dipoles can be curved by both blue- and red-detuned beams. The launched vortex dipoles can also be accelerated and decelerated by Gaussian beams with time-dependent intensity. Using two vortex-dipole launchers, we demonstrate collisions of vortex dipoles.

The present paper is organized as follows. Section II provides the formulation and numerical method. Section III studies vortex dipole generation by a red-detuned beam and shows that it can launch a vortex dipole in a controlled manner. Section IV investigates dynamics for two laser beams. Section V proposes methods to manipulate launched vortex dipoles and demonstrate their collisions. Section VI gives conclusions to this study.

II. FORMULATION OF THE PROBLEM

We consider a zero-temperature BEC in the mean-field approximation. The dynamics of the macroscopic wave function Ψ is described by the Gross-Pitaevskii (GP) equation given by

$$i\hbar \frac{\partial \Psi}{\partial t} = -\frac{\hbar^2}{2m} \nabla^2 \Psi + [V(x, y, t) + V_z(z)] \Psi + \frac{4\pi\hbar^2 a}{m} |\Psi|^2 \Psi, \quad (1)$$

where m is the atomic mass, V and V_z are the external potentials, and a is the s -wave scattering length. We assume that the system is tightly confined in the z direction and the confinement energy is much larger than other energy scales of the system. The wave function is thus frozen into $\Psi(x, y, z, t) = \psi(x, y, t) e^{iE_0 t/\hbar} \psi_0(z)$, where $\psi_0(z)$ and E_0 are the ground state and its energy for $V_z(z)$. Multiplying $\psi_0(z)$ to Eq. (1) and integrating it with respect to z , we reduce the 3D GP equation to

2D as

$$i\hbar \frac{\partial \psi}{\partial t} = -\frac{\hbar^2}{2m} \nabla_{\perp}^2 \psi + V(x, y, t) \psi + g|\psi|^2 \psi, \quad (2)$$

where ∇_{\perp}^2 is the 2D Laplacian and $g = 4\pi\hbar^2 am^{-1} \int |\psi_0|^4 dz$ is the effective interaction parameter in 2D space. We normalize the 2D wave function as $\tilde{\psi} = n_0^{-1/2} \psi$, where n_0 is the 2D atomic density in the absence of V . Normalizing the length and time by $\xi = \hbar/(mgn_0)^{1/2}$ and $\tau = \xi/v_s = \hbar/(gn_0)$, where $v_s = (gn_0/m)^{1/2}$ is the sound velocity, Eq. (2) is rewritten as

$$i \frac{\partial \tilde{\psi}}{\partial \tilde{t}} = -\frac{1}{2} \tilde{\nabla}_{\perp}^2 \tilde{\psi} + \tilde{V} \tilde{\psi} + |\tilde{\psi}|^2 \tilde{\psi}, \quad (3)$$

where the tilde represents normalized quantity. From this normalization, we find that the scaling law holds for the mean-field approximation. For example, the dynamics for the interaction strength gn_0 with a Gaussian potential $V = V_0 \exp\{-(x-vt)^2 + y^2\}/d^2\}$ and that for αgn_0 with $V = \alpha V_0 \exp\{-(x - \sqrt{\alpha}vt)^2 + y^2\}/(d/\sqrt{\alpha})^2\}$ obey the same equation (3) for an arbitrary constant $\alpha > 0$.

In the numerical simulations, we first prepare the ground state for $V(x, y, t = 0)$ by the imaginary time propagation of Eq. (3), i.e., i is replaced by -1 on the left-hand side of Eq. (3). We then add a small white noise to the ground state to break the exact numerical symmetry. Starting from this initial state, we obtain the time evolution by solving Eq. (3). The imaginary and real time propagation is calculated by the pseudospectral method, and therefore the periodic boundary condition is imposed. We take a large enough space in the simulations so that the boundary does not affect the dynamics.

III. VORTEX GENERATION BY A RED-DETUNED GAUSSIAN BEAM

A. Flow around a moving potential

First, we consider a single Gaussian laser beam moving through the condensate, which produces a potential as

$$V(x, y, t) = V_0 \exp \left[-\frac{(x + vt)^2 + y^2}{d^2} \right], \quad (4)$$

where d is the $1/e$ width of the laser beam. We assume that the laser beam moves in the $-x$ direction with the velocity v . The constant V_0 is proportional to the intensity of the laser beam, which is positive for blue detuning and negative for red detuning with respect to the resonant frequency of the electric dipole transition of atoms. The detuning is large and the heating of atoms by the spontaneous emission is negligible.

Frisch *et al.* [11] showed that quantized vortex dipoles are created around a moving rigid disk ($V = +\infty$ inside a disk) above a critical velocity. The vortex and antivortex are created at the lateral sides of the disk, and they

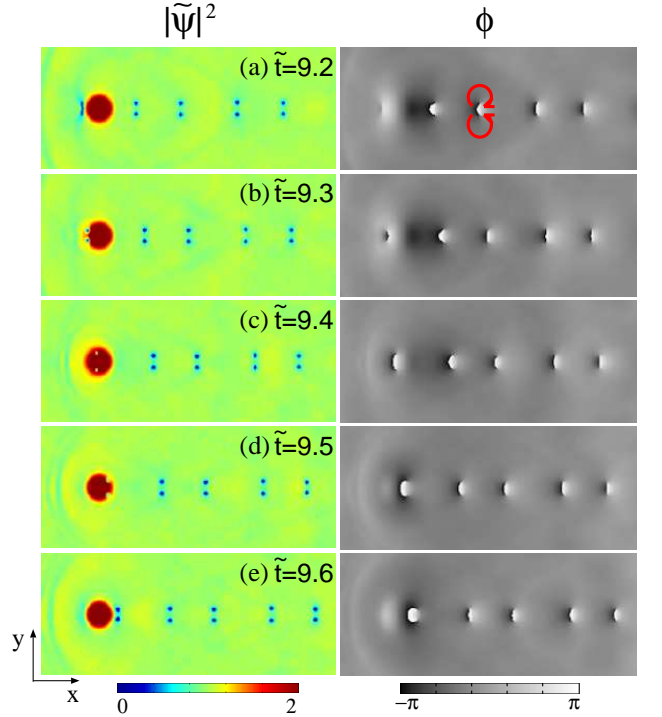


FIG. 1: Dynamics of the density $|\tilde{\psi}|^2 = |\psi|^2/n_0$ and phase $\phi = \arg \psi$ profiles for the Gaussian potential with $V_0/(gn_0) = -5$, $v/v_s = 0.6$, and $d/\xi = 4.5$ in the frame comoving with the potential. The arrows indicate the directions of circulations. The field of view of each panel is $160\xi \times 67\xi$.

are released into the wake (see Fig. 1 of Ref. [11]). The Gaussian potential (4) for $V_0 > 0$ also exhibits similar behavior [13, 15].

By contrast, we investigate the dynamics for a red-detuned ($V_0 < 0$) moving Gaussian beam, which is shown in Fig. 1. First, a density dip appears at the head of the potential [Fig. 1 (a)], which splits into vortex and antivortex [Fig. 1 (b)]. The vortex pair then passes through the potential avoiding the high density region [Fig. 1 (c)], and it is released behind the potential. The released vortex dipole moves in the $-x$ direction with the velocity $\hbar/(ml) = v_s \xi/l$, where l is the distance between the vortex and antivortex. Such vortex dynamics are repeated and vortex dipoles are shed in the wake periodically. The train of vortex dipoles is dynamically unstable and eventually sinuous destabilization spreads it in the $\pm y$ directions [17, 22]. In contrast to the case of a blue-detuned Gaussian beam, the Bénard-von Kármán vortex street [17] was not found for a red-detuned beam to the best of our investigation.

For an attractive potential ($V_0 < 0$), a vortex dipole is nucleated at the head of a moving potential, whereas a vortex dipole is nucleated at the lateral sides for a repulsive potential ($V_0 > 0$). To understand these behaviors, we consider the irrotational flow of an inviscid and incompressible fluid around a rigid disk. The velocity field

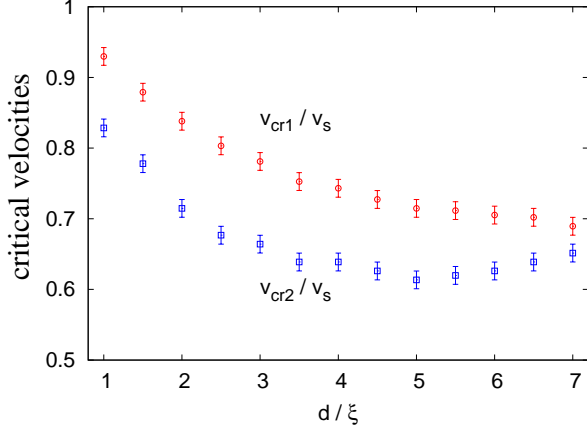


FIG. 2: Critical velocities for vortex dipole creation versus beam waist d of a moving red-detuned Gaussian beam. When the velocity of the beam is adiabatically increased, the vortex dipole creation occurs at v_{cr1} (circles). When the velocity of the beam is adiabatically decreased, the vortex dipole creation stops at v_{cr2} (squares). The intensity of the Gaussian potential (4) is fixed to $V_0/(gn_0) = -5$.

in the frame comoving with the disk is given by [23]

$$v_x - iv_y = U \left(1 - \frac{R^2}{r^2} e^{-2i\theta} \right), \quad (5)$$

where U and R are the velocity and radius of the disk, $r = (x^2 + y^2)^{1/2}$, and $\theta = \arg(x + iy)$. The velocity becomes maximum at $(r, \theta) = (R, \pm\pi/2)$, which agree with the locations at which vortices are nucleated. This is because vortices are nucleated when the velocity exceeds the local Landau critical velocity. Moreover, the density is low where the velocity is large due to Bernoulli's law and a quantized vortex with a density hole is easy to be nucleated.

For a disk-shaped strong attractive potential, where the density inside the disk n_{in} is much larger than the outside density n_{out} , the inside velocity must vanish in the limit of $n_{in}/n_{out} \rightarrow \infty$ since the normal component of the flow must be continuous across the boundary, $n_{in}v_{in}^\perp = n_{out}v_{out}^\perp$. Therefore, the tangential component of the velocity v^\parallel must vanish at the boundary, since it must be continuous. Such velocity field outside the disk is given by

$$v_x - iv_y = U \left(1 + \frac{R^2}{r^2} e^{-2i\theta} \right). \quad (6)$$

The velocity becomes maximum at $r = R$ and $\theta = 0, \pi$, and thus a vortex dipole is nucleated at the head of a potential. Perturbations at the tail of a potential ($r = R$ and $\theta = 0$) do not grow because they go downstream away.

It is interesting to note that the system exhibits hysteresis behavior with respect to the velocity. When the velocity of the beam is adiabatically increased from zero,

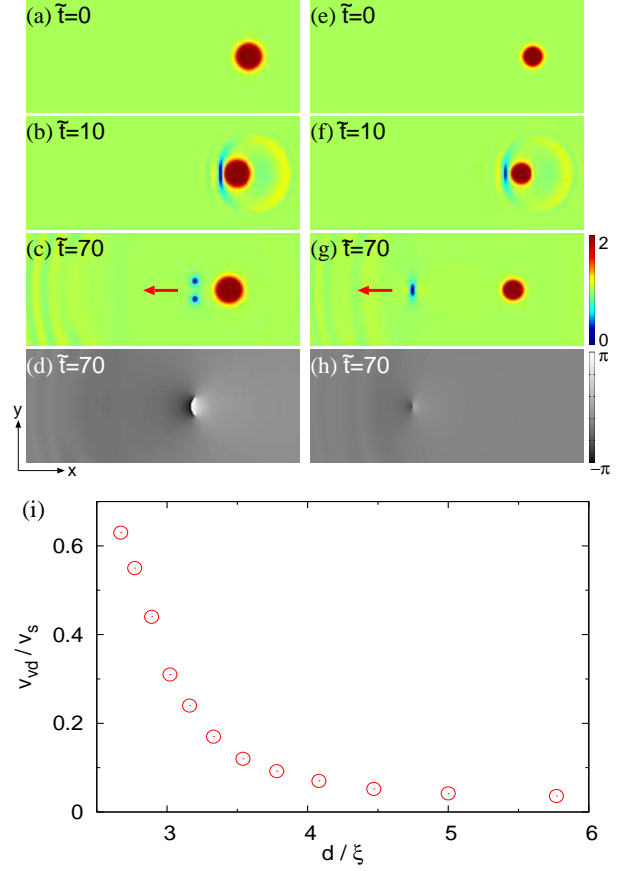


FIG. 3: (a)-(h) Snapshots of the density $|\psi|^2/n_0$ and phase $\phi = \arg\psi$ profiles in the rest frame. A Gaussian potential with $V_0/(gn_0) = -5$ is moved as in Eq. (7) with $v_0/v_s = 0.47$ and $T/\tau = 17$. The beam waist is $d/\xi = 3.54$ in (a)-(d) and $d = 2.67$ in (e)-(h). The arrows in (c) and (g) indicate the traveling direction of the vortex dipoles. The field of view of each panel is $78\xi \times 33\xi$. (i) Velocity of the launched vortex dipole versus beam waist d . The parameters except d are the same as those in (a)-(h).

the successive vortex dipole creation starts at a critical velocity v_{cr1} , which is shown by the circles in Fig. 2. On the other hand, when the velocity of the beam is decreased from $v > v_{cr1}$, the vortex dipole generation does not stop at $v = v_{cr1}$. The velocity v_{cr2} (squares in Fig. 2) at which the vortex dipole generation stops is slower than v_{cr1} . For the velocity $v_{cr2} < v < v_{cr1}$, the stationary flow remains to be stationary, and the successive vortex dipole creation is kept once it is triggered by perturbations.

B. Launching a vortex dipole

Using a red-detuned Gaussian laser beam, we can launch vortex dipoles in a controlled manner. The initial state is the ground state for the Gaussian potential in Eq. (4) with $V_0 < 0$ and $v = 0$. The potential then starts to move in the $-x$ direction at $t = 0$ and stops at $t = T$

as

$$v = \begin{cases} 0 & (t < 0, t > T) \\ v_0 & (0 \leq t \leq T) \end{cases}. \quad (7)$$

Figures 3 (a)-3 (h) show launching dynamics of a vortex dipole in the rest frame. After the stop of the potential, the created vortex dipole is released from the potential and continues to move in the $-x$ direction. Figures 3 (e)-3 (h) show the case of a smaller potential, in which a vortex dipole is bound so tight that the topological defects cannot be discerned [Fig. 3 (h)]. Such a solitonic structure is referred to as a rarefaction pulse [27], which has been shown to be formed by a local depletion [28] and an oscillating potential [21]. The rarefaction pulse propagates faster than the vortex dipole [Figs. 3 (c) and 3 (g)]. Figure 3 (i) shows the dependence of the velocity v_{vd} of the launched vortex dipole on the beam waist d . Since the distance between the created vortex and antivortex increases with an increase in the size of the potential, the velocity of the vortex dipole is a decreasing function of the size of the potential. Thus, the vortex dipole can be launched with controlled velocity.

IV. VORTEX GENERATION BY MULTIPLE GAUSSIAN BEAMS

A. Flow around double beams

We next consider the case of multiple Gaussian potentials. For simplicity, we assume that two identical Gaussian potentials move at the same velocity as

$$V = V_0 \sum_{j=1}^2 \exp \left[-\frac{(x - x_j + vt)^2 + (y - y_j)^2}{d^2} \right]. \quad (8)$$

The positions of the potentials are, without loss of generality, $(x_j, y_j) = (\mp \frac{D}{2} \sin \chi, \pm \frac{D}{2} \cos \chi)$ with the upper signs for $j = 1$ and the lower signs for $j = 2$, where the angle χ determines the alignment of the potentials.

Figure 4 shows a typical dynamics for two blue-detuned ($V_0 > 0$) beams with $\chi = 0$. The initial state is the ground state for $v = 0$ and the potentials start to move in the $-x$ direction at $t = 0$. After the initial disturbance, the system exhibits periodic behavior. A vortex dipole is created between the potentials and released in the wake [circle in the left panel of Fig. 4 (a)] with its counterpart being remained in the potentials [circles in the right panel of Fig. 4 (a)]. Then, the topological defects remained in the potentials are released from both ends [Fig. 4 (c)], and this dynamics is repeated. We note that small vortex dipoles released from between the potentials propagate in the x direction, whereas vortices in the outer rows propagate in the $-x$ direction [arrows in Fig. 4 (e)].

In order to understand the behavior in Fig. 4, we consider the irrotational flow of an inviscid and incompressible fluid around two rigid disks with radius $R > D/2$

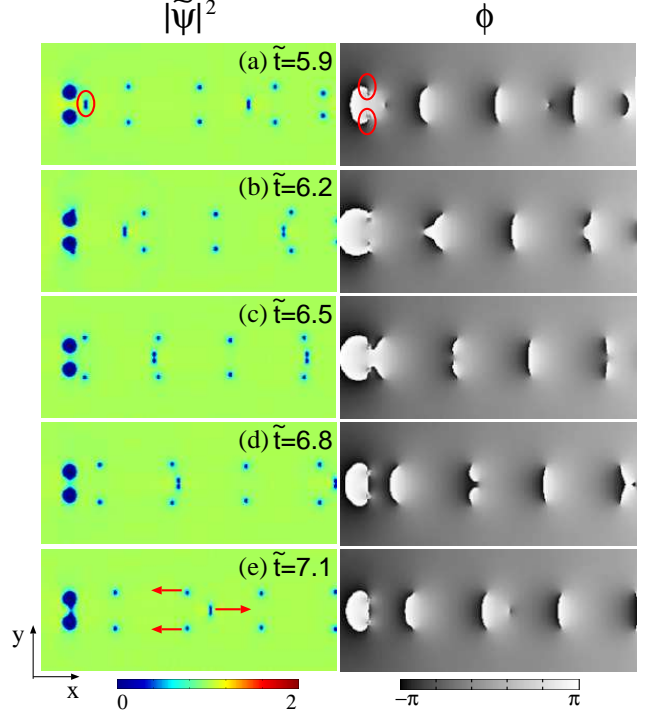


FIG. 4: Dynamics of the density $|\tilde{\psi}|^2 = |\psi|^2/n_0$ and phase $\phi = \arg \psi$ profiles for two Gaussian potentials with $V_0/(gn_0) = 100$, $d/\xi = 1.58$, $v/v_s = 0.35$, and $D/\xi = 12.6$ in the frame comoving with the potential. The circle in the left panel of (a) indicates a vortex dipole released from between the potentials, and those in the right panel its counterpart remained in the potentials. The arrows in (e) indicate the directions in which the vortices propagate. The field of view of each panel is $160\xi \times 67\xi$.

located at $(x, y) = (\mp \frac{D}{2} \sin \chi, \pm \frac{D}{2} \cos \chi)$. The velocity field is given by [24–26]

$$v_x - iv_y = \frac{4U \sinh^2 \beta}{(z/R)^2 + \sinh^2 \beta} \left[e^{i\chi} \wp(i\tau - i\beta) + e^{-i\chi} \wp(i\tau + i\beta) + \frac{2}{\pi} \zeta(\pi) \cos \chi \right], \quad (9)$$

where $\beta = \cosh^{-1}[D/(2R)]$, $z = x + iy$, $\tau = \beta + \log(ie^{-i\chi}z/R + \sinh \beta) - \log(ie^{-i\chi}z/R - \sinh \beta)$, and \wp and ζ are Weierstrass's elliptic functions with half periods π and $i \cosh^{-1}[(D^2/R^2 - 2)/2]$. The velocity field (9) approaches to $v_x - iv_y = U$ for $|z| \rightarrow \infty$. For $\chi = 0$, which corresponds to the case in Fig. 4, the velocity field in Eq. (9) is maximum at the inner edges of the disks. We denote the maximum velocity as $v_{\max} \equiv v_x(x = 0, y = \pm D/2 \mp R)$. The contour plot in Fig. 5 shows v_{\max} as a function of the distance D between the disks and the unperturbed velocity U . The maximum velocity v_{\max} monotonically decreases with an increase in D and linearly increases with an increase in U .

In Fig. 5, we superimpose the plots of the critical velocity v_{cr} for vortex dipole creation, obtained from the

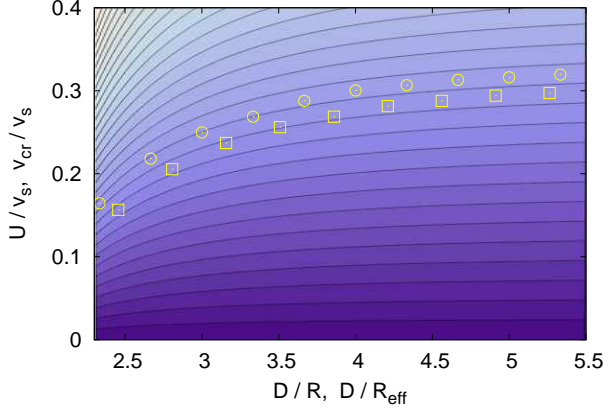


FIG. 5: Contour lines show the maximum velocity v_{\max} as a function of D/R and U/v_s , obtained from Eq. (9). The contour lines indicate $v_{\max}/v_s = 0.05, 0.1, 0.15, 0.2, \dots$ from below. The plots show the critical velocity v_{cr} for vortex dipole nucleation versus D/R_{eff} , which is obtained by simulations as in Fig. 4. Here R_{eff} is the radius of the density hole produced by the potential. The beam waist and the effective radius are $(d/\xi, R_{\text{eff}}/\xi) = (5, 9.5)$ for the circles and $(10, 18)$ for the squares.

GP equation (3) numerically. In the time evolution, we adiabatically increase the velocity v of the potential from $v = 0$ until a vortex dipole is nucleated as in Fig. 4, which determines the critical velocity v_{cr} . From Fig. 5, we find that the plots roughly fit the contour lines, implying that a vortex dipole is nucleated when the maximum velocity between the disks exceeds a local critical velocity, which is almost independent of D .

B. Launching a vortex dipole

Using two blue-detuned Gaussian beams, we can launch a vortex dipole, as in the case of a red-detuned beam in Sec. III B. The initial state is the ground state in the presence of two Gaussian potentials (8) with $V_0 > 0$, $v = 0$, and $\chi = 0$. The potentials are then displaced as in Eq. (7). Figures 6 (a)-6 (c) show the launching dynamics in the rest frame. A vortex dipole is generated between the potential and moves in the direction opposite to that of the displacement of the potentials. A vortex dipole is thus launched by “pulling” the potential, which is in contrast to the case of a red-detuned beam, in which a vortex dipole is launched by “pushing” the potential. After the launch, a counterpart of the released vortex-antivortex pair remains at the potential [dashed circle in Fig. 6 (d)], which prevents the successive launch. By contrast, the successive launch is possible for a red-detuned beam.

Figure 6 (e) shows the dependence of the velocity v_{vd} of a launched vortex dipole on the distance D between the two Gaussian potentials. The velocity v_{vd} decreases with an increase in D , since the distance between the

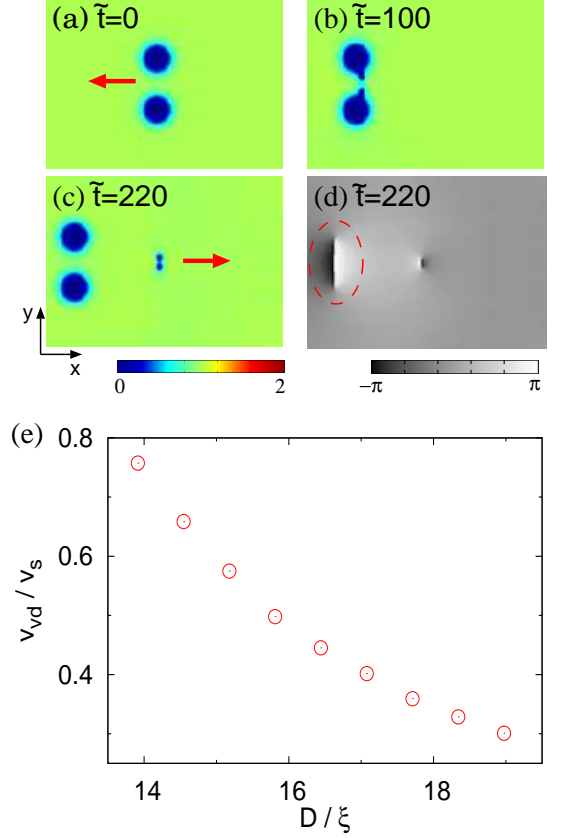


FIG. 6: (a)-(c) Dynamics of the density profiles $|\psi|^2/n_0$ for two Gaussian potentials with $V_0/(gn_0) = 5$, $d/\xi = 4.5$, and $D/\xi = 19$ in the rest frame. The potentials are moved as in Eq. (7) with $v_0/v_s = 0.24$ and $T/\tau = 133$. The arrows in (a) and (c) indicate the direction of the displacement of the potentials and that of the propagation of the vortex dipole, respectively. (d) Phase profile, $\arg\psi$, at $\tilde{t} = t/\tau = 220$. The topological defects in the dashed circle are the counterpart of the launched vortex dipole. The field of view of each panel is $90\xi \times 65\xi$. (e) Velocity of the launched vortex dipole versus distance D between the two Gaussian potentials. The parameters except D are the same as those in (a)-(d).

launched vortex and antivortex increases.

C. Trapping of a vortex dipole

We consider the dynamics for two red-detuned beams as shown in Fig 7. The initial state is the ground state for two Gaussian potentials in Eq. (8) with $V_0 < 0$, $v = 0$, and $\chi = 0$ [Fig 7 (a)] and the potentials start to move in the $-x$ direction at $t = 0$. Initially, the sudden increase in the velocity disturbs the system and several vortex dipoles are generated near the potential [Fig 7 (b)]. The vortex generation is only at the starting, and the generated vortex dipoles depart from the potential except the one between the potentials. Interestingly, this vortex dipole is trapped between the potentials and oscillates

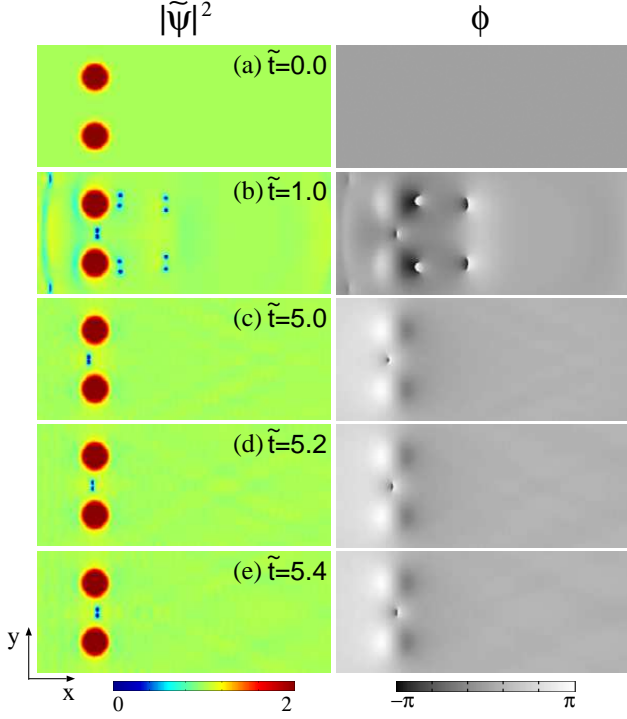


FIG. 7: Dynamics of the density $|\tilde{\psi}|^2 = |\psi|^2/n_0$ and phase $\phi = \arg\psi$ profiles for the potential in Eq. (8) with $V_0/(gn_0) = -5$, $v/v_s = 0.6$, $d/\xi = 4.5$, and $D/\xi = 31.6$ in the frame comoving with the potential. The field of view of each panel is $160\xi \times 67\xi$.

around the center in the moving frame [Figs 7 (c)-7 (e)].

In order to understand the trapping of a vortex dipole between moving potentials as shown in Fig. 7, we perform linear stability analysis assuming inviscid, incompressible, and irrotational flow. We consider the problem in the frame comoving with the potentials. Two point vortices with circulations $-h/m \equiv -\kappa$ and κ are located at $(x_1, y_1) = (\xi_1, l/2 + \eta_1)$ and $(x_2, y_2) = (\xi_2, -l/2 + \eta_2)$, where ξ_1 , η_1 , ξ_2 , and η_2 are small deviations from the stationary state and l is the distance between the vortex and antivortex for the stationary state. Equations of motion for the deviations are given by ($j = 1, 2$)

$$\dot{\xi}_j = v_x(x_j, y_j) - \frac{\kappa}{2\pi} \frac{y_1 - y_2}{r^2}, \quad (10a)$$

$$\dot{\eta}_j = v_y(x_j, y_j) + \frac{\kappa}{2\pi} \frac{x_1 - x_2}{r^2}, \quad (10b)$$

where $r^2 = (x_1 - x_2)^2 + (y_1 - y_2)^2 = (\xi_1 - \xi_2)^2 + (l + \eta_1 - \eta_2)^2$. The first terms on the right-hand side of Eq. (10) are the velocity field without the point vortices and the second terms are the velocity field produced by the other point vortex. We impose the same boundary condition as in Eq. (6) at $x^2 + (y \pm D/2)^2 = R^2$, giving the velocity

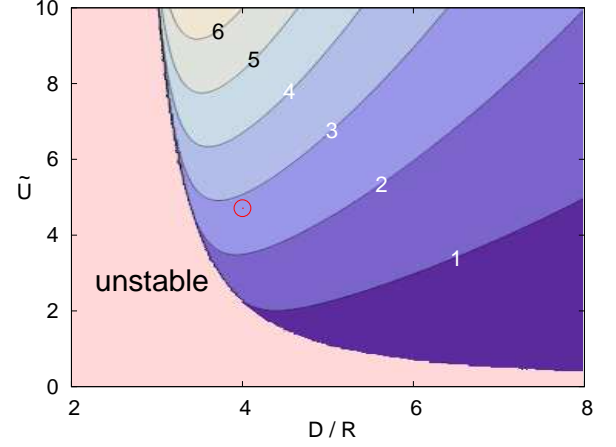


FIG. 8: Stability of a trapped vortex dipole with respect to the distance D between the potentials and the normalized velocity $\tilde{U} = 2\pi RU/\kappa$. When λ in Eq. (13) is real, the system is dynamically unstable. The contour plot shows $2\pi R^2|\lambda|/\kappa$ where λ is pure imaginary. The circle corresponds to the case in Fig. 7.

field without the point vortices as

$$v_x - iv_y = \frac{4U \sinh^2 \beta}{(z/R)^2 + \sinh^2 \beta} [\wp(i\tau - i\beta) - \wp(i\tau + i\beta)], \quad (11)$$

where β and τ are defined in Sec. IV A. Substituting Eq. (11) into Eq. (10) and neglecting the second and higher orders of the small deviations, we have

$$\dot{\xi}_1 = v_0 - c\eta_1 - \frac{\kappa}{2\pi} \left(\frac{1}{l} - \frac{\eta_1 - \eta_2}{l^2} \right), \quad (12a)$$

$$\dot{\eta}_1 = -c\xi_1 + \frac{\kappa}{2\pi} \frac{\xi_1 - \xi_2}{l^2}, \quad (12b)$$

$$\dot{\xi}_2 = v_0 + c\eta_2 - \frac{\kappa}{2\pi} \left(\frac{1}{l} - \frac{\eta_1 - \eta_2}{l^2} \right), \quad (12c)$$

$$\dot{\eta}_2 = c\xi_2 + \frac{\kappa}{2\pi} \frac{\xi_1 - \xi_2}{l^2}, \quad (12d)$$

where $v_0 = v_x(0, \pm l/2)$ and $c = -\partial_y v_x(0, l/2) = \partial_y v_x(0, -l/2) = -\partial_x v_y(0, l/2) = \partial_x v_y(0, -l/2)$. In order for the point vortices to be stationary at $(0, \pm l/2)$, we set $v_0 = \kappa/(2\pi l)$, which determines l for given U , D , and R . Equations (12) then become homogeneous differential equations and have the solutions of the form $\xi_j, \eta_j \propto e^{\lambda t}$. The eigenvalues λ are obtained as

$$\lambda = \pm \sqrt{c^2 - \frac{c\kappa}{\pi l^2}}. \quad (13)$$

If the eigenvalues are pure imaginary, i.e., $c < \kappa/(\pi l^2)$ the solutions are oscillatory and the two point vortices are stable. If $c > \kappa/(\pi l^2)$, the small deviations grow exponentially and the system is dynamically unstable.

Figure 8 shows a contour plot of $|\lambda|$ in Eq. (13) for the stable region. The stable trapping dynamics shown in

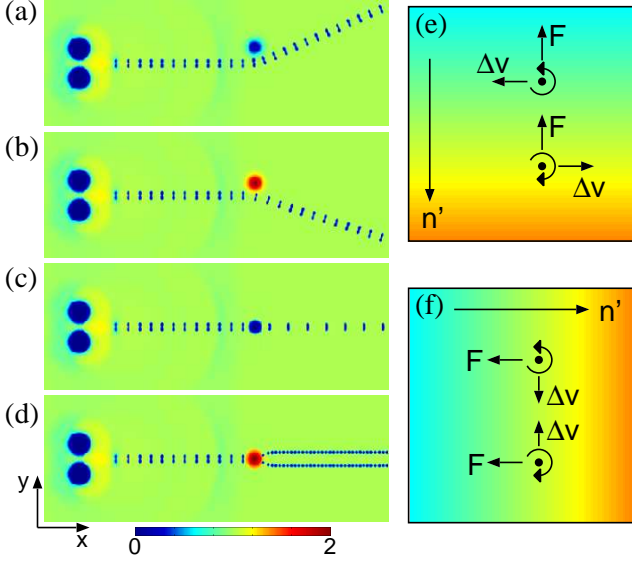


FIG. 9: Stroboscopic images of the density profile $|\psi|^2/n_0$ in the rest frame. A vortex dipole is launched by the two Gaussian potentials as in Fig. 6 with $V_0/(gn_0) = 5$, $d/\xi = 4.5$, and $D/\xi = 19$. The stroboscopic images are taken at time intervals of $\Delta t/\tau = 20$. (a) A Gaussian potential with $V_0/(gn_0) = 1$ and $d/\xi = 4.5$ is located at $y = 1.6$. (b) A Gaussian potential with $V_0/(gn_0) = -1$ and $d/\xi = 4.5$ is located at $y = 1.6$. (c) A Gaussian potential with $V_0/(gn_0) = 1$ and $d/\xi = 4.5$ is switched on at $t/\tau = 330$. (d) A Gaussian potential with $V_0/(gn_0) = -1$ and $d/\xi = 4.5$ is switched on at $t/\tau = 330$. The field of view of each panel is $224\xi \times 80\xi$. (e), (f) Schematic illustrations for explaining the Magnus effect.

Fig. 7 corresponds to the circle in Fig. 8. From Fig. 8, we find that $|\lambda|$ increases with an increase in U and the trapping is tight for large U . However, if U exceeds the critical velocity, vortex dipoles are successively generated from the potentials as in Fig. 1, which disturbs the trapping. Therefore, there is an appropriate region of D and U for the most efficient trapping.

V. MANIPULATION OF VORTEX DIPOLES

We next show that the velocity and trajectory of a launched vortex dipole can be changed after the launch. We use a static Gaussian potential to curve trajectories of vortex dipoles, and use a time-dependent Gaussian potential to accelerate and decelerate them. Figure 9 shows stroboscopic images of such dynamics. A vortex dipole is launched in the same manner as in Fig. 6. In Fig. 9 (a), a weak repulsive Gaussian potential is located near the trajectory of the vortex dipole and the trajectory bends toward the potential. In Fig. 9 (b), the obstacle potential is attractive and the trajectory bends in the opposite direction. In Fig. 9 (c), a repulsive Gaussian potential is switched on at the moment that the vortex dipole passes through, which accelerates the vortex dipole. In Fig. 9

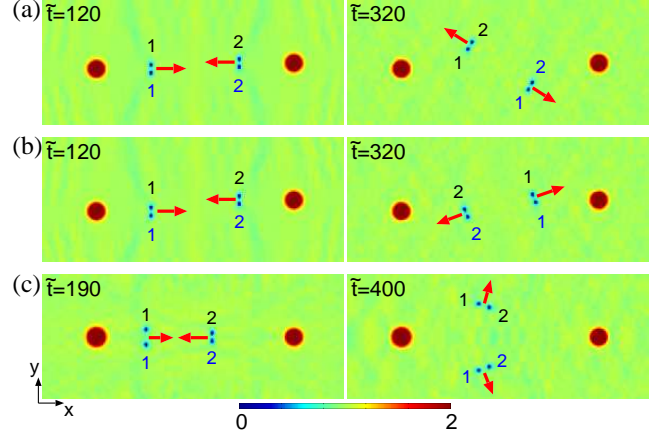


FIG. 10: Collisions between vortex dipoles launched by the method in Fig. 3. The directions in which the vortex dipoles propagate are indicated by the arrows. The numbers and their colors identify the vortices. (a) Collision with the impact parameter $b/\xi = 3.16$. Vortex exchange occurs. (b) Collision with $b/\xi = 6.32$. The two vortex dipoles pass each other. (c) Collision of vortex dipoles with different velocities. The beam waist is $d/\xi = 3.54$ for the left-hand side in (c) and $d/\xi = 3.16$ for the others. The other parameters are the same as those in Fig. 3. The field of view of each panel is $78\xi \times 33\xi$.

(d), on the other hand, an attractive potential is switched on and the vortex dipole is decelerated.

The behaviors in Figs. 9 (a)-9 (d) can be understood by the Magnus effect. The Magnus force on each vortex is given by $\mathbf{F}_M = mn\boldsymbol{\kappa} \times \Delta\mathbf{v}$, where $\boldsymbol{\kappa}$ is the vector of circulation and $\Delta\mathbf{v}$ is the velocity relative to the unperturbed velocity of the vortex dipole. When force \mathbf{F} is exerted on a vortex, the velocity changes in such a way that \mathbf{F} balances with \mathbf{F}_M , and hence

$$\Delta\mathbf{v} = \frac{1}{mn\kappa^2} \boldsymbol{\kappa} \times \mathbf{F}. \quad (14)$$

In Fig. 9, the origin of the force is the density gradient produced by the obstacle Gaussian potential. The energy of a vortex is roughly given by $E \sim \pi\hbar^2 n/m$ and the force on a vortex is $\mathbf{F} \sim -\pi\hbar^2 \nabla n/m$, which is in the direction opposite to the density gradient. Two examples of the effect of density gradient on a vortex dipole are shown in Figs. 9 (e) and 9 (f). When the density gradient is perpendicular to the traveling direction of a vortex dipole [rightward for Fig. 9 (e)], its trajectory is curved toward the direction of $-\nabla n$, which explains the dynamics in Figs. 9 (a) and 9 (b). When a vortex dipole propagates in the direction of ∇n as in Fig. 9 (f), the distance between the two vortices decreases and the vortex dipole accelerates. This corresponds to the situation in Fig. 9 (c), where a density dip suddenly appears just behind the vortex dipole. The deceleration in Fig. 9 (d) can also be understood in a similar manner.

Using the method to launch vortex dipoles, we demonstrate collisions between two counter-propagating vortex dipoles. The two vortex dipoles are launched in the $\pm x$

directions by red-detuned Gaussian beams as in Fig. 3. Figures 10 (a) and 10 (b) show collisions between two vortex dipoles launched with the same velocity. When the “impact parameter” b is small, each vortex in the two vortex dipoles are exchanged, and the two vortex dipoles with new pairs go away with the same scattering angle [Fig. 10 (a)]. The scattering angle is $\pi/2$ for frontal collision ($b = 0$, data not shown). In Fig. 10 (b), the impact parameter is large and the two vortex dipoles pass each other without vortex exchange. Figure 10 (c) shows collision between vortex dipoles with different velocities, where the vortex exchange occurs and the new vortex dipoles scatter with scattering angles φ and $\pi - \varphi$. This is understood from the momentum conservation, where a slower vortex dipole (larger distance between vortices) has a larger momentum [18]. Collisions between point vortex dipoles in classical fluids have been studied in Refs. [29, 30].

VI. CONCLUSIONS

We have investigated dynamics of a 2D BEC stirred by far-off-resonant Gaussian laser beams. When a red-detuned beam (attractive potential) moves through a BEC exceeding a critical velocity, a vortex dipole is nucleated at the head of the moving potential (Fig. 1). This is in contrast to a blue-detuned (repulsive) beam, in which a vortex dipole is generated on both sides of the potential. The vortex shedding from a red-detuned beam exhibits the hysteresis behavior with respect to the velocity (Fig. 2). When a red-detuned beam is displaced, a created vortex dipole propagates towards the direction of the displacement, which can be used as a “vortex-dipole

launcher” (Fig. 3). When two repulsive potentials are moved, a vortex dipole is generated between the potentials, which propagates to the direction opposite to the motion of the potential (Fig. 4). A vortex dipole can also be launched by two blue-detuned beams (Fig. 6). The velocity of vortex dipoles can be controlled in the two launching methods. For two red-detuned beams, we found that a vortex dipole can be trapped between two moving potentials (Fig. 7). Launched vortex dipoles can be manipulated by an external potential (Fig. 9). A trajectory of a vortex dipole is curved by a Gaussian potential located near the trajectory. A Gaussian potential with time-dependent intensity on the trajectory of a vortex dipole can change its velocity.

We have thus shown that we can create and launch vortex dipoles in a controlled manner and also manipulate their trajectories and velocities after the launch. These are achieved only by a quasi-2D BEC and Gaussian laser beams. This technique enables us to investigate a variety of dynamics of quantized vortices in superfluids, such as collisions of vortex dipoles (Fig. 10).

Acknowledgments

This work was supported by Grants-in-Aid for Scientific Research (No. 20540388, No. 22340116, No. 23540464, and No. 23740307) from the Ministry of Education, Culture, Sports, Science and Technology of Japan, and Japan Society for the Promotion of Science. T. Kishimoto thanks for Special Coordination Funds for Promoting Science and Technology (Highly Talented Young Researcher) from Japan Science and Technology Agency.

-
- [1] V. L. Berezinskii, Sov. Phys. JETP **34**, 610 (1972)
 - [2] J. M. Kosterlitz and D. J. Thouless, J. Phys. C **6**, 1181 (1973).
 - [3] L. Onsager, Nuovo Cimento Suppl. **6**, 249 (1949).
 - [4] R. P. Feynman, *Progress in Low Temperature Physics*, vol. 1, ed. C. J. Gorter (North-Holland, Amsterdam, 1955).
 - [5] S. Inouye, S. Gupta, T. Rosenband, A. P. Chikkatur, A. Görlitz, T. L. Gustavson, A. E. Leanhardt, D. E. Pritchard, and W. Ketterle, Phys. Rev. Lett. **87**, 080402 (2001).
 - [6] G. Roumpos, M. D. Fraser, A. Löffler, S. Höfling, A. Forchel, and Y. Yamamoto, Nature Phys. **7**, 129 (2011).
 - [7] T. W. Neely, E. C. Samson, A. S. Bradley, M. J. Davis, and B. P. Anderson, Phys. Rev. Lett. **104**, 160401 (2010).
 - [8] D. V. Freilich, D. M. Bianchi, A. M. Kaufman, T. K. Langin, and D. S. Hall, Science **329**, 1182 (2010).
 - [9] S. Middelkamp, P. J. Torres, P. G. Kevrekidis, D. J. Frantzeskakis, R. Carretero-González, P. Schmelcher, D. V. Freilich, and D. S. Hall, arXiv:1104.0092.
 - [10] P. Kuopanportti, J. A. M. Huhtamäki, and M. Möttönen, Phys. Rev. A **83**, 011603(R) (2011).
 - [11] T. Frisch, Y. Pomeau, and S. Rica, Phys. Rev. Lett. **69**, 1644 (1992).
 - [12] T. Winiecki, J. F. McCann, and C. S. Adams, Phys. Rev. Lett. **82**, 5186 (1999).
 - [13] T. Winiecki, B. Jackson, J. F. McCann, and C. S. Adams, J. Phys. B **33**, 4069 (2000).
 - [14] A. Aftalion, Q. Du, and Y. Pomeau, Phys. Rev. Lett. **91**, 090407 (2003).
 - [15] B. Jackson, J. F. McCann, and C. S. Adams, Phys. Rev. Lett. **80**, 3903 (1998).
 - [16] C. Nore, C. Huepe, and M. E. Brachet, Phys. Rev. Lett. **84**, 2191 (2000).
 - [17] K. Sasaki, N. Suzuki, and H. Saito, Phys. Rev. Lett. **104**, 150404 (2010).
 - [18] M. Crescimanno, C. G. Koay, R. Peterson, and R. Walsworth, Phys. Rev. A **62**, 063612 (2000).
 - [19] J. S. Stieβberger and W. Zwerger, Phys. Rev. A **62**, 061601 (2000).
 - [20] C. Huepe and M. E. Brachet, Physica D **140**, 126 (2000).
 - [21] K. Fujimoto and M. Tsubota, Phys. Rev. A **82**, 043611 (2010).
 - [22] C. Nore, M. E. Brachet, and S. Fauve, Physica D **65**, 154

- (1993).
- [23] See, for example, H. Lamb, *Hydrodynamics*, 6th ed (Dover, New York, 1945).
 - [24] W. M. Hicks, Quart. J. Pure Appl. Math. **16**, 113 (1879).
 - [25] A. G. Greenhill, Quart. J. Pure Appl. Math. **18**, 356 (1882).
 - [26] D. G. Crowdy, Eur. J. Mech. B / Fluids **25**, 459 (2006).
 - [27] C. A. Jones and P. H. Roberts, J. Phys. A **15**, 2599 (1982).
 - [28] N. G. Berloff, Phys. Rev. B **65**, 174518 (2002).
 - [29] S. V. Manakov and L. N. Shchur, JETP Lett. **37**, 54 (1983).
 - [30] B. Eckhardt and H. Aref, Phil. Trans. Roy. Soc. Lond. A **326**, 655 (1988).